ASEAN Engineering Journal

Full Paper

GREEN SYNTHESIS, CHARACTERISTICS, ANTIMICROBIAL ACTIVITY AND ANTIOXIDANT OF NANO SILVER USING RED FLESH DRAGON FRUIT (*HYLOCEREUS POLYRHIZUS*) PEEL EXTRACT

Van-Son Nguyen*, Thai Viet Hung, Vo Thanh Cong, Van Thnah Khue

Faculty of Chemical Engineering, Industrial University of Ho Chi Minh City, Ho Chi Minh City, Viet Nam

Article history
Received
8 December 2024
Received in revised form
15 May 2025
Accepted
29 May 2025
Published online
28 February 2026

*Corresponding author
nguyenvanson@iuh.edu.vn

Graphical abstract

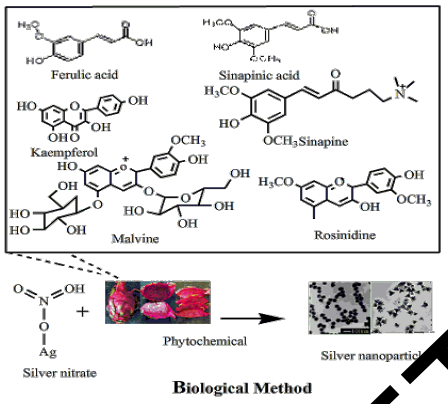

Abstract

Green nanosynthesis is increasingly attracting scientists to research and discover. In this study, we have successfully synthesized nano silver from Red flesh Dragon fruit (Hylocereus polyrhizus) peel extract. The clean and safe nano synthesis can both solve the problem of organic waste in the processing industry, and can provide silver nanoparticles for different application purposes, especially in antibacterial, antifungal and medical. The nanoparticles have been morphologically and structurally characterized by modern physicochemical analysis methods: Fourier Transform Infrared Spectroscopy (FT-IR), Dynamic Light Scattering (DLS), X-ray Diffraction (XRD), Scanning Electron Microscopy (SEM) and Transmission Electron Microscopy (TEM). The characteristics of Silver nanoparticles are shown on XRD spectrum with angle 2θ = 38.24°, 44.28°, 64.48° and 77.38°. The average nanoparticle size through TEM images was in the range of 20-100 nm. Moreover, silver nanoparticles have been evaluated for their antibacterial ability on *Escherichia coli, Klebsiella pneumoniae, Staphylococcus aureus, Bacillus subtilis*, and antioxidant by ABTS method. The testing process shows that they have very good resistance to oxidation and bacteria. It holds promise for a potential antioxidant and antibacterial application.

Keywords: Green synthesis, AgNPs, Antibacterial, Antioxidat, Red flesh Dragon fruit

1.0 INTRODUCTION

Silver is a precious metal known for its outstanding electrical conductivity and ductility. Additionally, it is biocompatible, making it highly suitable for medical applications, particularly due to its strong antimicrobial properties [1]. Compared to conventional silver, silver nanoparticles (AgNPs) exhibit enhanced efficiency owing to their significantly smaller size and larger specific surface area, which increase their chemical reactivity and biological activity [2]. Research has demonstrated that AgNPs possess superior antibacterial effects compared to traditional silver-based compounds [3]. As a result, AgNPs have been widely applied in various industries, including electronics, biosensors, biomedical materials, catalysis, household disinfectants, water purification systems, and cosmetics, mainly due to their broad-spectrum antimicrobial properties [4–7].

The synthesis of AgNPs has attracted significant research interest, leading to the development of multiple fabrication techniques. Methods such as ultraviolet irradiation, photochemical reduction, electrochemical reduction, and reverse micelle techniques have been utilized to produce AgNPs with uniform morphology and controlled size distribution [8–11]. The antibacterial effectiveness of AgNPs is strongly dependent on their particle size, with smaller nanoparticles exhibiting greater antimicrobial potential [12,13]. Notably, liquid-phase reduction techniques have demonstrated significant promise in synthesizing AgNPs with excellent antibacterial properties, making them highly relevant for biomedical and industrial applications [14].

In recent years, green synthesis approaches, particularly those using plant extracts as reducing and stabilizing agents, have gained substantial attention. These eco-friendly methods are favored due to their simplicity, cost-effectiveness, and minimal environmental impact. Moreover, they enable the production of biocompatible nanoparticles suitable for various medical and industrial applications [15]. For instance, AgNPs

synthesized using melon extract have displayed notable insecticidal properties [16], while those synthesized from Azadirachta indica extract have demonstrated superior photocatalytic and antibacterial performance compared to pure AgCl materials [17]. Additionally, tea extract has been successfully used as a reducing and stabilizing agent in AgNP synthesis, with the resulting nanoparticles exhibiting antimicrobial effects against Escherichia coli and Pseudopestalotiopsis theae [18]. Similarly, AgNPs synthesized using Kalanchoe pinnata (life plant) extract have shown antibacterial activity against gram-negative E. coli and photocatalytic efficiency in degrading rhodamine B dye [19].

Despite these advancements, synthesizing AgNPs using plant extracts presents certain challenges, particularly in achieving consistent particle size distribution and uniformity. Consequently, ongoing research focuses on optimizing synthesis parameters to enhance particle size control and reproducibility [20].

Red flesh dragon fruit (Hylocereus polyrhizus), illustrated in Figure 1, belongs to the Cactaceae family and is widely cultivated across tropical regions. Native to Mexico and Colombia, this species was introduced to Vietnam approximately 50–60 years ago, with historical accounts indicating its arrival during the French colonial era [21]. Traditionally, red flesh dragon fruit has been valued for its mildly sweet or sour taste and its various health benefits, including cooling effects, lung support, expectorant properties, and cholesterol reduction [22]. The fruit is also rich in antioxidants, which play a crucial role in combating oxidative stress. Predominantly grown in southern Vietnam, red flesh dragon fruit is an important agricultural export, with an annual production exceeding one million tons. However, the large volume of discarded peels contributes to environmental pollution [23].

Red flesh dragon fruit peels contain bioactive compounds such as quercetin, betacyanin, flavonoids, and organic acids, which exhibit antibacterial and antioxidant properties [24]. Utilizing these peels for AgNP synthesis presents a dual advantage: it offers an environmentally sustainable approach to waste management while serving as a cost-effective source of nanoparticles with potential applications in biomedical and industrial fields.

Figure 1 Ingredients of Red flesh dragon fruit (*Hylocereus polyrhizus)*

2.0 METHODOLOGY

2.1 Materials And Chemicals

2.1.1 Chemicals

In this study, red flesh dragon fruit used for the extraction and synthesis of silver nanoparticles was sourced from Ham Thuan Nam District, Binh Thuan Province, and was collected in February 2023. The selection criteria ensured that the fruit had a uniform color (red or pink) with no burnt spikes or signs of pest damage. The silver ion (Ag^+) solution was prepared using silver nitrate ($AgNO_3$) obtained from Sigma-Aldrich. All other chemicals used in the experiments were of analytical grade

2.1.2 Machine Equipment

UV-Vis spectroscopy was employed to characterize and determine the optical density of silver nanoparticles using a Thermo Gensys 10 spectrophotometer (190–1100 nm), with water as the solvent. FT-IR analysis (FT-IR-4700) was conducted to identify organic functional groups in the dragon fruit peel extract, which served as both a silver nanoreducing agent and a colloidal stabilizer. XRD analysis (Bruker D8 Advance, Cu Kα) was performed over a 2θ range of 10–80°. Particle size and zeta potential were measured using Horiba's SZ-100 Analyzer, while morphology was examined using Fe-SEM (Hitachi S-4800) and TEM (JEM 1010) in ethanol or water.

2.2 Prepare the Extract

After the flesh was removed from the dragon fruit, the peel was dried at 70 °C until a constant weight was reached, then cut into small pieces. A 5 g portion of the dried peel was combined with 400 mL of deionized distilled water as the solvent. The mixture was heated to boiling and maintained at a simmer for 1 hour. After the extraction process was completed, the solution was filtered using Whatman filter paper (Cat. No. 1001-110) to remove any residual solid peel. Since water served as the solvent, the extract was freshly prepared for each experimental session. A concentrated portion of the extract was subsequently analyzed for its chemical composition using LC-MS chromatography.

2.3 Synthesis of AgNPs

To synthesize silver nanoparticles (AgNPs), a 50 mL solution containing Ag^+ ions at concentrations ranging from 0.5 to 4 mM was first prepared. Then, 50–250 mL of red-fleshed dragon fruit peel extract was added to the reaction mixture. The pH was adjusted to 8 using a 3% NaOH solution. Various reaction parameters, including reaction time, mixture ratio, Ag^+ concentration, temperature, and reaction medium, were optimized for AgNP synthesis, as illustrated in Figure 2.

The resulting AgNP solution was filtered using Whatman filter paper (Cat. No. 1001-110) to remove larger particles and subsequently centrifuged at 10,000 rpm. The solid precipitate was washed multiple times with deionized distilled water, then collected and dried under vacuum to obtain the silver nanoparticles in solid form, as illustrated in Figure 7

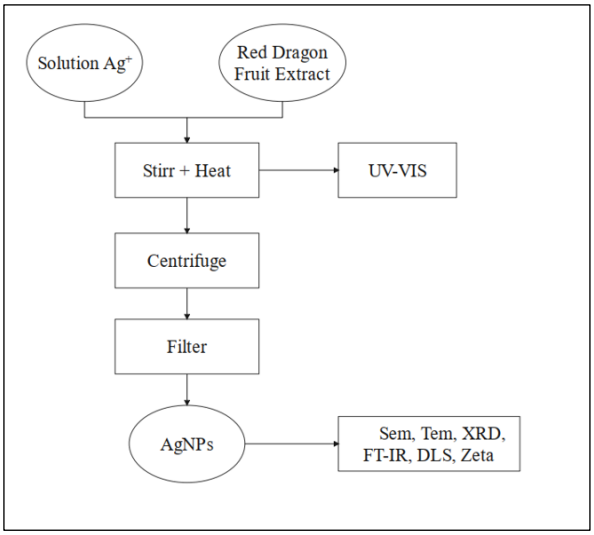

Figure 2 Synthesis process of AgNPs

2.4 Investigation of Free Radical Scavenging by ABTS

The antioxidant capacity of AgNPs was evaluated using the $ABTS^{\bullet+}$ free radical scavenging method. The $ABTS^{\bullet+}$ solution was prepared by mixing 20 μL of ABTS stock solution (7 μM) with 2.45 μM $K_2S_2O_8$ and allowing the reaction to proceed in a dark flask for 12–24 hours. The resulting solution was then diluted with ethanol and analyzed using UV-Vis spectroscopy at 734 nm, ensuring an absorbance of 0.7 ± 0.02. A 25 μL aliquot of AgNPs solution (at concentrations of 50, 100, 200, 300, and 400 μM) was added to 3 mL of the $ABTS^{\bullet+}$ solution. After one minute, the absorbance was measured at 734 nm. Trolox was used as a positive control for calibration at concentrations of 50, 100, 200, 300, and 400 μM.

2.5 Test Antibacterial

The Ag nanoparticle samples synthesized under optimal conditions were diluted into four smaller samples with decreasing concentrations as follows:
- Sample 1: 5 μL optimized Ag nano solution.
- Sample 2: 3.5 μL single-phase sample with 15 μL CH_3OH.
- Sample 3: 2 μL of single-phase sample with 30 μL of CH_3OH.
- Sample 4: 0.5 μL single-phase sample with 45 μL CH_3OH.

The mixed samples were absorbed onto filter paper and dried, forming 6 mm holes for antibacterial testing. Sterile distilled water was used to mix the bacterial culture, which was then spread onto the agar surface using a cotton swab. The prepared samples were subsequently placed on the agar surface, and the plates were incubated at 34.9 °C for 24 hours. To determine the antibacterial diameter of the nanosamples, a blank sample was included on each plate as a control solvent. Sample layout diagram on agar plate: B: Blank; A1: Sample 1; Sample 2; Sample 3 and Sample 4, as shown in Figure 3.

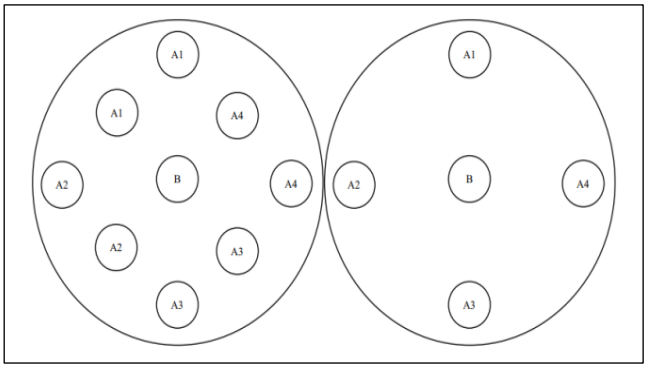

Figure 3 Antibacterial layout diagram

3.0 RESULTS AND DISCUSSION

3.1 Chemical Composition of Dragon Fruit Peel Extract by LC-MS

The red flesh dragon fruit peel extract contains a variety of bioactive compounds, including flavonoids, betacyanins, polyphenols, and organic acids, as identified through LC-MS analysis (Table 1). These compounds play a crucial role in the reduction and stabilization of Ag^+ ions during AgNP synthesis. Based on the molecular weights observed in the LC-MS spectra, several of these compounds have been tentatively identified and are listed in Table 1, providing insight into the specific phytochemicals potentially responsible for nanoparticle formation and stabilization.

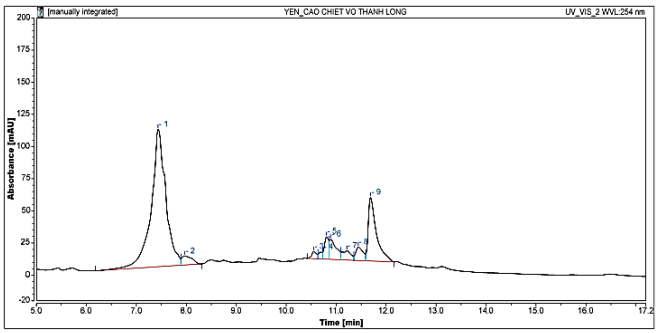

Figure 4: Results of liquid chromatography-mass spectrometry (LC-MS) of Red flesh Dragon fruit peel extract at UV-VIS_2WVL 254 nm

Flavonoids, a major class of polyphenolic compounds, are known for their antioxidant and metal-chelating properties, which facilitate the reduction of Ag^+ to Ag^0, thereby promoting nanoparticle formation. Additionally, betacyanins, a group of natural pigments abundant in dragon fruit peels, act as both reducing agents and capping agents, preventing nanoparticle aggregation and enhancing their stability. Organic acids, such as ascorbic acid and citric acid, contribute to the synthesis process by modulating pH and further aiding in the reduction of silver ions.

The presence of these bioactive components not only supports the green synthesis of AgNPs but also enhances their antibacterial and antioxidant properties, making them suitable for biomedical and environmental applications.

Table 1 Prediction and identification of some active ingredients in Red flesh Dragon fruit martial extracts based on LC/MS spectrum on Figure 4.

No.	Compounds name	Molecular formula	Structural formula
1	Ferulic acid	$C_{10}H_{10}O_4$	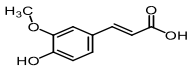
2	Sinapinic acid	$C_{11}H_{12}O_5$	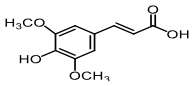
3	Kaempferol	$C_{15}H_{10}O_6$	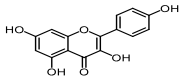
4	Sinapine	$C_{16}H_{24}NO_5^+$	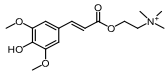
5	Cyanidine	$C_{15}H_{11}O_6^+$	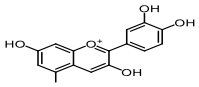
6	Quercetine	$C_{15}H_{10}O_7$	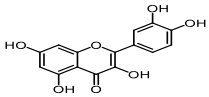
7	Malvine	$C_{29}H_{35}O_{17}^+$	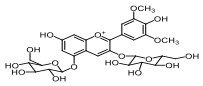
8	Flavane	$C_{15}H_{14}O$	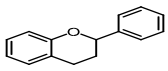
9	Rosinidine	$C_{17}H_{15}O_6^+$	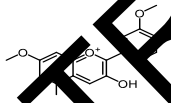

3.2. Mechanism of Ag Nanofabrication from Red flesh Dragon Fruit Extract

The extract of red flesh dragon fruit contains various bioactive components, as summarized in Table 1, including flavonoids and organic acids with hydroxyl (OH) groups attached to aromatic rings. These OH groups in polyphenols play a critical role in the reduction of Ag^+ ions to silver nanoparticles (AgNPs) through the following general mechanism, where R represents an aromatic ring-containing group.

This mechanism suggests that phenolic compounds in flavonoids, organic acids with aromatic rings, and other constituents of red dragon fruit peel extract function as reducing agents, facilitating the conversion of Ag^+ ions into elemental silver (Ag). At lower pH levels, the high concentration of H^+ ions shifts the reaction equilibrium (Equation 1) from right to left, thereby decreasing the reaction rate (Equation 2) and reducing the efficiency of Ag^+ reduction to Ag. Conversely, at higher pH levels, the reaction rate (Equation 2) increases, leading to enhanced synthesis of Ag nanoparticles, as illustrated in Figure 5. This mechanism is consistent with the optimal conditions for AgNP formation, which occur at a pH of 8.

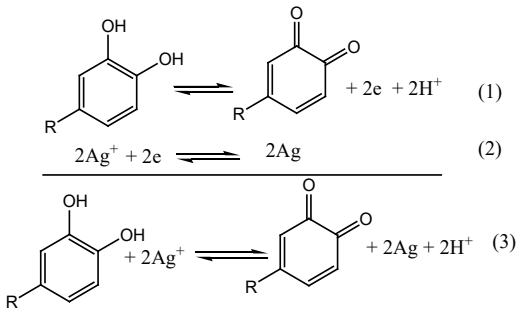

Figure 5 Mechanism of redox reaction of Red flesh Dragon fruit peel extract and solutions Ag^+

3.3 Research on Factors Affecting the Synthesis of AgNPs

As the concentration of $AgNO_3$ increased from 0.001 M to 0.002 M, a steady rise in optical density was observed, with the absorbance reaching a peak value (A_{max}) of 3.201 at a wavelength (λ_{max}) of 449 nm (Figure 6a). The distinct absorption band within the 425–520 nm range is indicative of the successful synthesis of silver nanoparticles (AgNPs), as it corresponds to their characteristic surface plasmon resonance (SPR). The enhanced absorbance at 0.002 M suggests a higher nanoparticle yield, highlighting this concentration as the most favorable among the tested levels.

Beyond this point, however specifically at concentrations exceeding 0.003 M a decline in absorbance was detected. This reduction may be attributed to nanoparticle aggregation, which can occur when increased precursor availability accelerates reaction kinetics, resulting in uncontrolled particle growth and clustering. Moreover, the limitations of the UV-Vis spectrophotometer at high concentrations may also contribute to underestimating absorbance values. Such outcomes emphasize the importance of maintaining a balanced precursor concentration to prevent aggregation and ensure reliable spectroscopic detection.

A similar pattern was observed when varying the ratio of plant extract to $AgNO_3$. Increasing the extract-to-metal ion ratio from 1:1 to 2:1 led to a corresponding increase in optical density, with the maximum absorbance (A_{max} = 2.47) recorded at 440 nm (Figure 6b). This enhancement likely reflects the greater availability of bioactive compounds in the extract, which play a key role in reducing Ag^+ ions and stabilizing the formed nanoparticles. The 2:1 ratio thus appears optimal for supporting effective nanoparticle synthesis. Conversely, further increasing the ratio to 3:1 resulted in a notable reduction in absorbance intensity. This outcome is possibly due to an excess of organic constituents that may overcoat the nanoparticle surfaces, promoting agglomeration and reducing colloidal stability ultimately causing the UV-Vis peak to fade or disappear.

Temperature also played a critical role in AgNP formation. UV-Vis spectra revealed that at lower temperatures (30–40 °C), no significant absorption peak was present, suggesting insufficient reducing capacity under mild thermal conditions. As the temperature rose from 40 °C to 80 °C, a gradual increase in absorbance was noted, indicating that elevated temperatures enhanced reduction kinetics and nanoparticle nucleation, leading to the formation of well-dispersed particles. The temperature of 80 °C proved particularly effective, as it balanced reaction speed with particle stability, producing the most intense and well-defined SPR signal.

However, at 90 °C, a decrease in absorbance occurred, likely due to increased particle aggregation. At this higher thermal threshold, excessive Brownian motion and weakened interactions between nanoparticles and stabilizing agents in the extract may have promoted fusion via mechanisms such as Ostwald ripening or sintering. The resulting formation of larger aggregates with diminished surface area accounts for the observed decline in optical density.

Collectively, these findings confirm that the optimal synthesis conditions for AgNPs included a 0.002 M Ag^+ concentration, a 2:1 extract-to-metal ion ratio, a reaction temperature of 80 °C, and a reaction time of 60 minutes. Under these parameters, silver nanoparticle formation was most efficient, yielding stable colloidal dispersions with strong surface plasmon resonance signatures.

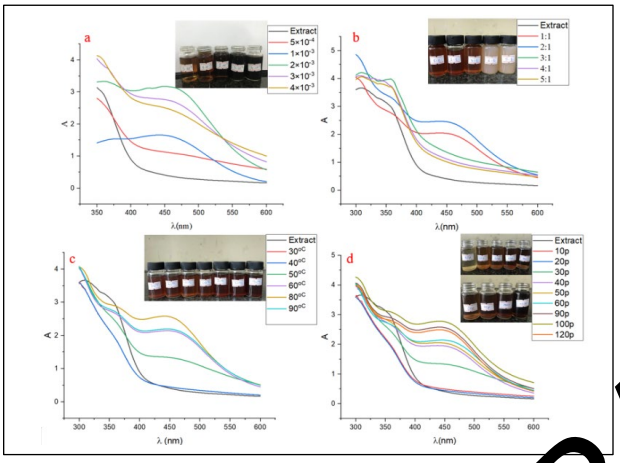

Figure 6: a/ UV-VIS spectrum to investigate the concentration of $AgNO_3$ b/ UV-VIS spectrum to investigate the ratio of extract - $AgNO_3$ / UV-Vis spectroscopy was utilized to investigate the temperature-dependent synthesis of silver nanoparticles. d/ UV-Vis spectroscopy was employed to analyze the time-dependent synthesis of silver nanoparticles.

The peaks of the UV-VIS spectrum we obtained are distributed mostly in the wavelength range fr[illegible]00-4[illegible]5 nm [illegible]g. Observing the results, we can see that the adsorption intensity of the obtained sample tends to incre[illegible]se gradually with the reaction time. However, if the reaction time is 100 minutes or more, the adsorption will decrease because the nanosystem becomes less stable over time. During the preservation of solutions containing Silver nanoparticles, we found that Ag nanosolutions synthesized at over 100 minutes coagulated very quickly. Therefore, in order to save time and energy, we have chosen to synthesize silver nano-solutions for 60 minutes. With the absorption peak at 447 nm with A_{max} = 2,147.

Figure 7 Liquid (left) and solid (right) samples of Nano Silver after synthesis under optimal conditions

3.4 The Results of Analysis of Structural Properties of Ag Nano Particles Using Physicochemical Methods

3.4.1 FTIR Infrared Absorption Spectrum of AgNPs

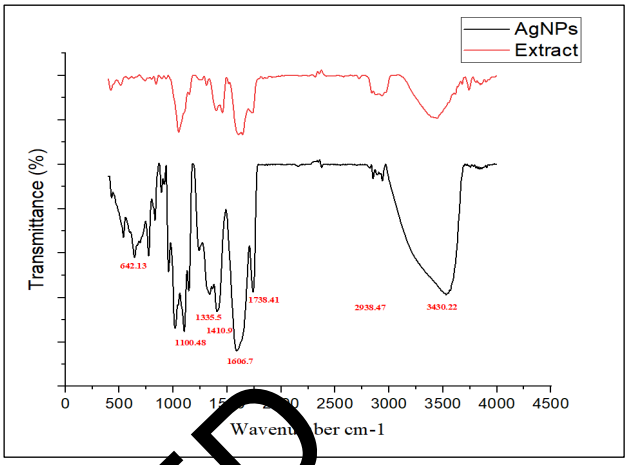

Figure 8: FT-IR infrared absorption spectrum of Silver nanoparticles

Moreover, the functional group of Red flesh Dragon fruit extract and silver nanoparticles was identified by FT-IR. The band of silver nanoparticles assigned at 3430 cm^{-1} might be corresponded to O-H stretching vibration, the peak at 2938 cm^{-1} corresponds to the contraction group of the C-H group in the aromatic nucleus, the peak around at 1738 cm^{-1} corresponds to C=O stretching vibration, the peak at 1606 cm^{-1} corresponds to the contraction group of Ag-O, while 1021 cm^{-1} corresponds to C-O phenolic compounds. Comparing with the band of silver nanoparticles, there are many infrared peaks of natural products in Red flesh Dragon fruit extracts, which might corresponding to different groups, such as C=C stretching vibration (1695 cm^{-1}), C-H deformation vibration (1452 cm^{-1}), and C-O stretching vibration (1044 cm^{-1}).

The oscillation frequency of Ag nanoparticles appeared spectral peaks at the wavelengths listed in Figure 8. The spectral peaks have changed compared to the extract of Red flesh Dragon fruit skin, especially new peaks appear at about 642 cm^{-1} and sharp peak at 1606 cm^{-1} representing the formed Ag^+-O functional group.

3.4.2. Spectrum XRD of AgNPs

The XRD spectrum of the AgNPs (Figure 9) displays four distinct characteristic peaks at 2θ angles of 38.24°, 44.28°, 64.48°, and 77.38°. These peaks correspond to the Miller indices (111), (200), (220), and (311), respectively, which are associated with the cubic crystal structure of silver nanoparticles (JCPDS file No. 04-0783) [24,25].

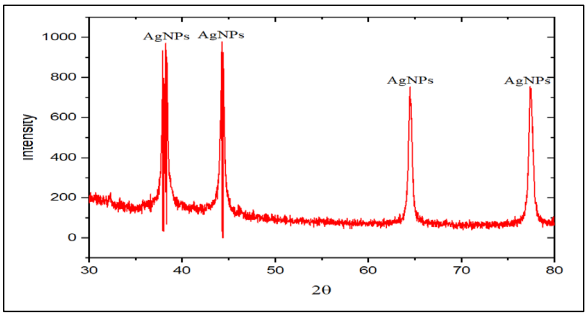

Figure 9 Spectrum XRD of AgNPs

3.4.3. DLS Particle Size Distribution and Zeta Potential

From the size analysis chart of Silver nanoparticles, we can see that the particle size distribution is mainly from 10-400 nm. The distributions are concentrated at 20-100 nm. There are also particles with a large size of 100-400 nm (Figure 10), this is because the organic substances in the extract enclose the nanoparticles, making them less agglomerate when in small concentrations, then the nanoparticles generate more can be agglomerated into larger clumps causing them to settle. The average silver nanoparticle size was 60.1 nm.

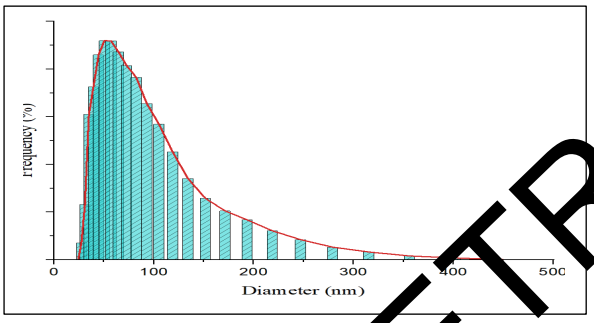

Figure 10 Particle size distribution of silver nanoparticles

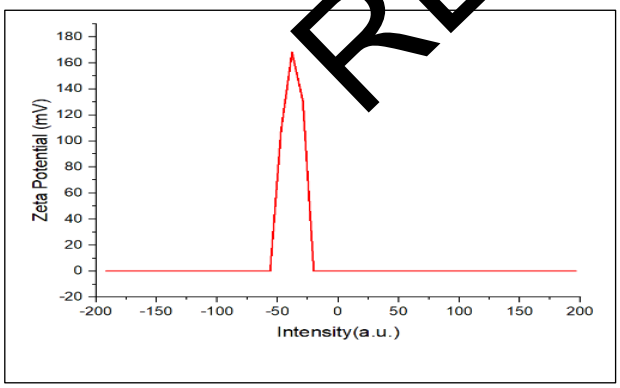

Figure 11 Spectral determination of the stability and distribution of Silver nanoparticles

Our silver nanosystem, synthesized under optimal conditions, has a Zeta potential of -38.158 mV (in Figure 11). This result indicates that the silver nanoparticles are stable and evenly dispersed within the colloidal system. The negative charge of the nanoparticles is likely due to the presence of OH^-, COO^-, and CO functional groups in the extract, as identified by FT-IR spectroscopy. These negative charges cause the nanoparticles to repel each other, preventing agglomeration and thus stabilizing the nanosystem, which enhances its overall efficiency.

3.4.4. SEM Image

The FE-SEM image (Figure 12) reveals that the synthesized silver nanoparticles (AgNPs) predominantly exhibit a quasi-spherical morphology with relatively smooth surfaces. The particles appear fairly well-defined, although a certain degree of aggregation is observed, which is commonly reported for biosynthesized or chemically reduced AgNPs due to high surface energy and interparticle van der Waals attractions.

Based on the 500 nm scale bar, the particle sizes are estimated to fall mainly within the nanoscale range of approximately 40–100 nm, with some variation in diameter. The size distribution appears moderately broad, suggesting that nucleation and growth processes may not have occurred entirely uniformly during synthesis. The presence of both smaller and slightly larger particles indicates overlapping stages of nucleation and subsequent particle growth.

Overall, the morphology and size range observed in the FE-SEM image confirm the successful formation of nanoscale silver particles, consistent with typical characteristics of AgNPs prepared via green or chemical reduction methods.

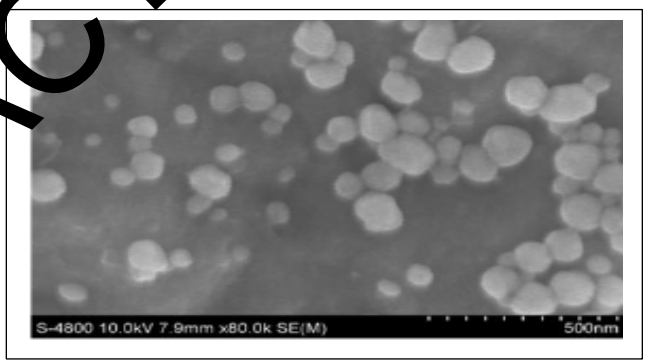

Figure 12 FE-SEM image of AgNPs at 500 nm magnifications

3.4.5 TEM Image

The TEM images of AgNPs synthesized under optimal conditions demonstrate a remarkably uniform particle size, primarily ranging between 20 and 100 nm (in Figure 13). The nanoparticles exhibit a predominantly spherical shape and are evenly dispersed throughout the solution. Following centrifugation, the particles were collected and redissolved in the solvent. TEM analysis revealed that the silver nanoparticles are encased in organic substances, contributing to an increase in particle size. This larger size can negatively impact the antibacterial properties of the sample. Additionally, the presence of these organic compounds likely explains the film formation observed when the solid AgNPs are dried.

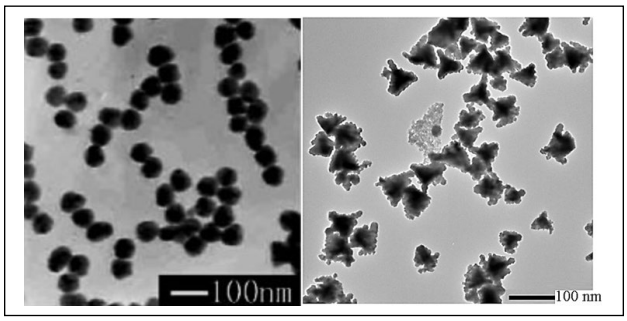

Figure 13 TEM images of Ag nano in solution and the form of particles (centrifugation to collect the particles and then dissolve in the solvent for measurement)

3.5. Test Results for Oxidation Resistance

3.5.1. Set Up The Standard Curve

Where inhibition is the percentage reduction in activity compared to the control. For more precise calculation, it's common to use software or graphical methods (in Figure 14) to determine IC_{50} from experimental data.

Table 2 Results of standard curve construction with Trolox solution

Trolox			
C(µM)	A_i	$SC_{ABTS^{\cdot+}}$	IC_{50} (μM)
50	0.686	2	
100	0.648	7.429	
200	0.598	14.571	8.41
300	0.552	21.143	
400	0.505	27.857	

So we can calculate IC_{50} as:

$$IC_{50} = \frac{50-b}{a} = \frac{50+5.0284}{6.5428} = 8.41 \ (\mu M)$$

Where: a and b are the coefficients in the equation y = ax+b.

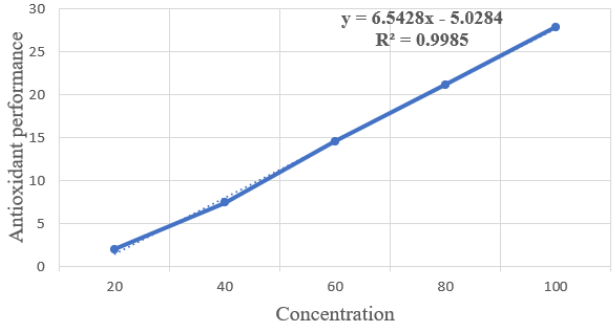

Figure 14 Trolox calibration curve used to determine $ABTS^{\cdot+}$ reduction capacity

From the experimental results, it can be seen that the antioxidative performance of Trolox also increases as its concentration increases. Specifically, when Trolox content increased from 50-400 μM, the antioxidant efficiency also increased to 2-27.857%. The $ABTS^{\cdot+}$ free radical scavenging capacity of Trolox is shown through the IC_{50} index, the results are shown in Table 2 and Figure 14, with IC_{50} = 8.41 μM.

3.5.2 Testing The Oxidation Resistance Of Nano Silver

Ag nanoparticle solution has IC_{50} value = 32.347 μg/mL, when increasing the concentration of nanoparticles in the solution from 50-400 μM, the antioxidant efficiency also increases. From the above results, it can be seen that the silver nano solution that we have synthesized has the ability to remove $ABTS^{\cdot+}$ free radicals very well (with IC_{50} value <100 μM). In comparison the oxidation resistance of standard trolox (IC_{50}=8.41 μM) was 3.85 times higher than that of the nano solution. We have summarized the results shown in Table 3 and on Figure 15.

Table 3 $ABTS^{\cdot+}$ free radical scavenging efficiency of AgNPs

AgNPs			
C(µM)	A	$SC_{ABTS^{\cdot+}}$	IC_{50} (μM)
50	0.699	0.143	
100	0.689	1.521	
200	0.678	3.184	32.347
300	0.666	4.885	
400	0.655	6.429	

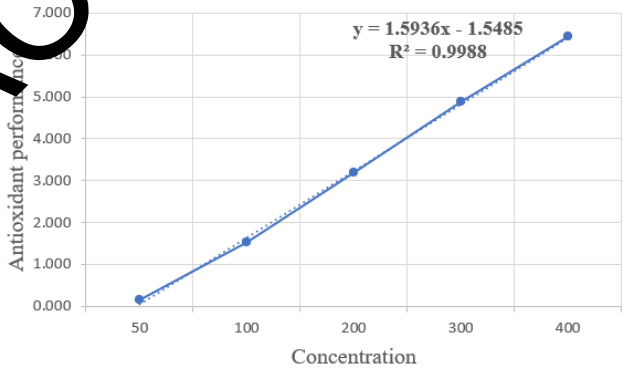

Figure 15 free radical scavenging ability of AgNPs by $ABTS^{\cdot+}$

3.4.3. Test results for Antibacterial Ability

From the results of the antibacterial activity, the silver nanoparticles with the size of 50 nm were resistant to 4 types of bacteria: Bacillus subtilis, Staphylococcus aureus (yellow staphylococcus), Esherichia coli and Klebsiella pneumoniae. With the antibacterial ring diameters listed in Table 4, we found that the antibacterial activity of AgNPs on rod-shaped bacteria (E.Coli and Bacillus) was better than on spherical bacteria (Klebsiella and Staphylococcus aureus). Spherical bacteria with R-plasmid gene can produce Penicillinase enzyme, besides it can also produce proteins that reduce the antibacterial activity of Nano Silver as on Figure 16 and in Table 4

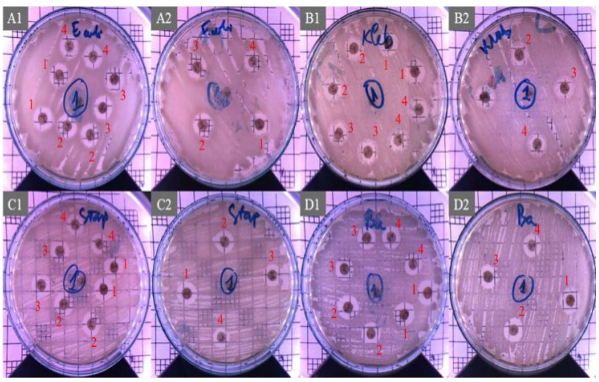

Figure 16 Test results of antibacterial activity of AgNPs solution

Table 4 Test results of antibacterial activity of AgNPs solutio

No.	Bacterial strain	Samples	Antibacterial Diameter (cm) 1st time	2nd time	3rd time	Medium
1	*Escherichia coli*	1	0.6	0.7	0.6	0.63
		2	0.6	0.7	0.6	0.63
		3	0.5	0.6	0.5	0.53
		4	0.4	0.4	0.5	0.43
2	*Klebsiella pneumoniae*	1	0.6	0.7	0.7	0.67
		2	0.5	0.6	0.5	0.53
		3	0.4	0.5	0.4	0.43
		4	0.3	0.4	0.4	0.37
3	*Staphylococcus aureus*	1	0.7	0.6	0.6	0.63
		2	0.6	0.6	0.6	0.60
		3	0.5	0.6	0.6	0.57
		4	0.4	0.5	0.5	[illegible]
4	*Bacillus subtilis*	1	0.8	0.8	0.8	[illegible]
		2	0.7	0.7	[illegible]	[illegible]
		3	0.6	0.6	0.6	0.60
		4	0.6	0.5	[illegible]	[illegible]

.

4.0 CONCLUSION

In this study, LC-MS analysis of red flesh dragon fruit peel extract identified compounds like Ferulic acid, Sinapinic acid, Kaempferol, and Quercetin, which can reduce Ag^+ ions to silver nanoparticles (AgNPs). The optimal synthesis conditions were a 0.002 M Ag^+ solution, a 2:1 extract-to-Ag^+ ratio, a reaction temperature of 80 °C, and a reaction time of 60 minutes. XRD, FT-IR, and Zeta potential analyses confirmed the composition and properties of the AgNPs, which were spherical with sizes ranging from 20 to 100 nm, as revealed by DLS, SEM, and TEM. The AgNP solution showed strong antioxidant activity (IC_{50} = 32.347 μM) and effective antibacterial action *against Bacillus subtilis, Staphylococcus aureus, Escherichia coli*, and *Klebsiella pneumoniae*, with inhibition zone diameters ranging from 0.63 to 0.8 mm. These results highlight the potential of AgNPs for antibacterial applications.

Acknowledgement

The authors thank the Industrial University of Ho Chi Minh City (IUH) for the facility support.

Conflicts of Interest

The author(s) declare(s) that there is no conflict of interest regarding the publication of this paper

References

[1] Jean-Yves Maillard, Philippe Hartemann. 2012. "Silver as an antimicrobial: Facts and gaps in knowledge." *Critical Reviews in Microbiology*, 39(4): 373–383. DOI: https://doi.org/10.3109/1040841X.2012.713323
[2] Pal, T.R.R., Singh, V.K., Kumar, M., Lee, S.R.C.R.S.Y.Y., Sundar, M.P.K., Kumar, R.K.S., Gupta, S.K. 2021. Size-dependent properties of silver nanoparticles and their applications in biomedical fields. *Nanomedicine: Nanotechnology, Biology and Medicine* 19: 12–21.
[3] Gupta, A.K., Sharma, S.M. 2020. Antibacterial and antifungal activities of silver nanoparticles synthesized using Azadirachta indica leaf extract. *Journal of Nanoparticle Research* 14: 564–571.
[4] Bhatia, R.V.K., Patel, S.S., Singh, A.K. 2019. Applications of silver nanoparticles in electronics and environmental science. *Nano Letters.* 20: 2158–2165.
[5] Park, J.L.P., Park, H.J., Lim, C.H. 2013. Use of silver nanoparticles in water filtration and air purification systems. *Water Research*. 47: 2283–2294.
[6] Smith, C.S., Johnson, E.R. 2017. Silver nanoparticles in textiles: Benefits and challenges. *Journal of Textile Science* 25: 73–85.
[7] Kim, H.S., Lee, Y.K., Hong, J.H. 2022. Silver nanoparticles in cosmetics: A review of their benefits and potential risks. *Cosmetic Science* 12: 45–52.
[8] Silva, M.S.C., Sanchez, D.A., Ribeiro, J.T. 2019. Photochemical methods for the synthesis of silver nanoparticles. *Chemistry of Materials.* 22: 1525–1530.
[9] Kim, L.E.T., Choi, H.J. 2018. Electrochemical synthesis of silver nanoparticles for medical applications. Journal of the Electrochemical Society. 165: B3089–B3096.
[10] Al-Badri, D.S., Khalid, T.B., Akhtar, S.E. 2021. Reverse micelle synthesis of silver nanoparticles: A comprehensive study. *Langmuir.* 37: 10298–10308.
[11] Deshmukh, N.G., Pandit, S.P. 2020. Ultraviolet-assisted synthesis of silver nanoparticles: Optimization and characterization. *Nanotechnology* 11: 1421–1429.
[12] Lee, Y.M., Jung, K.S., Park, A.H.R. 2019. Influence of particle size on the antibacterial activity of silver nanoparticles. *Journal of Nanomedicine.* 16: 56–67.
[13] Patil, R.K.S., Rana, A.S. 2015. Antibacterial efficacy of silver nanoparticles: Size and shape dependence. *Biomaterials.* 28: 3267–3276.
[14] Lee, M.S., Shin, D.H., Nam, E.J. 2016. Liquid reduction methods for synthesizing silver nanoparticles with antibacterial properties. *Nanomedicine: Nanotechnology, Biology and Medicine* 15: 983–992.
[15] Gomez, A.J., Smith, R.A. 2020. Green synthesis of silver nanoparticles using plant extracts: A review. *Journal of Cleaner Production* 243: 118640.
[16] Shah, P.N., Kumar, K.B., Bose, A.C.R. 2021. Insecticidal activity of silver nanoparticles synthesized using fresh melon extracts. *Pest Management Science.* 78: 1224–1232.
[17] Ali, S.S., Ali, M.R. 2020. Photocatalytic and antibacterial enhancement of silver nanoparticles synthesized using Azadirachta indica extract. *Catalysts.* 10: 671.
[18] Lee, K.T., Chung, M.H. 2021. Synthesis of silver nanoparticles using tea extract: Antimicrobial and antifungal properties. *Journal of Nanobiotechnology* 19, 26.
[19] Yu, J.C., Wang, X.Z., Chiu, M.R. 2021. Green synthesis of silver nanoparticles using Kalanchoe pinnata leaves and their application in dye degradation. *Environmental Science and Pollution Research,* 28: 25430–25441. DOI: doi.org/10.1016/j.cplett.2021.138760
[20] Brown, L.M.D., Sharma, R.N. 2021. Challenges in controlling particle size and distribution in plant extract-based nanoparticle synthesis. *Nanomaterials.* 11: 1886.
[21] Patel, R.K.M., Singh, G.K. 2020. Historical introduction and traditional uses of Hylocereus polyrhizus in Vietnam. *Journal of Ethnobiology and Ethnomedicine,* 16: 12.
[22] Park, J.H., Cho, L.Y. 2019. Traditional medicinal uses of red flesh dragon fruit (Hylocereus polyrhizus): Health benefits and properties. *Phytotherapy Research.* 33: 787–797.
[23] Kumar, A.S., Sethi, S.P. 2020. Environmental impact of red flesh dragon fruit cultivation and waste management. *Journal of Cleaner Production* 264: 121501.
[24] Meng, Y. 2015. A sustainable approach to fabricating Ag nanoparticles/PVA hybrid nanofiber and its catalytic activity. *Nanomaterials*. 5(2): 1124–1135.
[25] Priyadharshini, R.I., Geetha, G.P.N., Venkatachalam, P. 2014. Microwave-mediated extracellular synthesis of metallic silver and zinc oxide nanoparticles using macro-algae (Gracilaria edulis) extracts and its anticancer activity against human PC3 cell lines. *Applied Biochemistry and Biotechnology.* 174(8): 2777–2790. DOI: 10.1007/s12010-014-1225-3